

Confinement and critical regime in doped frustrated quasi-one dimensional magnets

NICOLAS LAFLORENCIE^{1,2}, DIDIER POILBLANC¹

¹ *Laboratoire de Physique Théorique, CNRS-UMR5152 Université Paul Sabatier, F-31062 Toulouse, France*

² *Department of Physics & Astronomy, University of British Columbia, Vancouver, B.C., Canada, V6T 1Z1*

Ground state and finite temperature properties of a system of coupled frustrated and/or dimerized spin-1/2 chains modeling e.g. the CuGeO₃ compound are reviewed. Special emphasis is put on the investigation of the role of impurity doping. A chain-mean field computation combining exact diagonalisations of the chain hamiltonians together with a mean field treatment of the weak interchain couplings is performed in order to map the microscopic model onto a low-energy effective model. The latter describes a 2-dimensional system of effective spin-1/2 local moments interacting by spacially anisotropic long range spin exchange interactions. An extensive study of this effective model is performed by Stochastic Series Expansion Quantum Monte Carlo for a wide range of temperatures and impurity concentrations. Interesting scaling behaviors of the uniform and staggered spin susceptibilities (above a small ordering Néel temperature due to a residual 3D coupling) can be interpreted in terms of the formation of large clusters of correlated spins carrying a finite magnetization. Such results are reproduced satisfactorily by a new Real Space RG enabling to deal with long range interactions in two-dimensions.

KEYWORDS: Strongly correlated systems, Quantum magnetism, Critical behaviors, Numerical simulations, Random magnets

1. Introduction

Low dimensional gapped quantum magnets have attracted a lot of interest in condensed matter physics for many years. The possibility of doping such systems has lead to an extremely rich emerging field. For instance, the discovery of the first non-organic spin-Peierls (SP) compound CuGeO₃¹ and its doping with static non-magnetic impurities realized by direct substitution of a small fraction of copper atoms by zinc² or magnesium³ atoms offered a new challenge for the theorist. Replacing a spin- $\frac{1}{2}$ in a *spontaneously* dimerized spin chain by a non-magnetic impurity, described as an inert site, releases a free spin- $\frac{1}{2}$, named a soliton, which does not bind to the dopant.⁴ The physical picture is completely different when a *static* bond dimerisation exists and produces an attractive potential between the soliton and the dopant^{4,5} and consequently leads, under doping, to the formation of local magnetic moments^{4,6} as well as a rapid suppression of the spin gap.⁷ However, a coupling to a purely one-dimensional (1D) adiabatic lattice⁸ does not produce confinement in contrast to more realistic models including an elastic inter-chain coupling (to mimic 2D or 3D lattices).^{8,9}

In the following, we are going to present through a generic model of quasi one-dimensional SP system the impurity induced local moment formation as well as the tendency towards antiferromagnetic (AF) ordering in the thermodynamic limit observed for any non-zero dopant concentration. An interesting low temperature scaling behavior will also be presented and interpreted in term of the formation of large clusters of correlated spins carrying a finite magnetization. This short review is the consequence of several previous works¹⁰⁻¹² involving many numerical tools: Lanczos Exact Diagonalization (ED) associated to chain-mean field theory, Stochastic Series Ex-

pansion (SSE) Quantum Monte Carlo (QMC) methods including long-range interactions, numerical Real Space Renormalization Group (RSRG) technique.

The rest of the paper is organized as follows. In the following section, we introduce a generic microscopic model describing weakly coupled frustrated spin- $\frac{1}{2}$ chains, and compute its phase diagram without impurity. Then in section 3 we concentrate on impurity effects, through the confinement mechanism, responsible of the impurity induced local moment formation. We also study the effective interaction between impurities which enable us to construct an effective two-dimensional (2D) diluted model. The section 4 is thus devoted to the impurity induced AF ordering which appear in such an effective model. Finally, in the section 5 we focus on the low temperature regime of the effective 2D model for which a RSRG procedure has been developed.

2. Microscopic model of coupled frustrated spin- $\frac{1}{2}$ chains

2.1 Generic Hamiltonian for weakly coupled spin-Peierls chains

We start with the microscopic Hamiltonian

$$\mathcal{H} = \sum_{a=1}^M \sum_{i=1}^L [J(1 + \delta_{i,a}) \vec{S}_{i,a} \cdot \vec{S}_{i+1,a} + \alpha J \vec{S}_{i,a} \cdot \vec{S}_{i+2,a} + h_{i,a} S_{i,a}^z], \quad (1)$$

as a generic model for a quasi one-dimensional frustrated spin system¹⁰ with J and α both positive, and $S = \frac{1}{2}$. i is a lattice index along the chain of size L and a labels the M chains. The effective magnetic field $h_{i,a}$ results from a mean-field (MF) treatment¹³ of a weak interchain coupling, $J_{\perp} \vec{S}_{i,a} \cdot \vec{S}_{i,a+1}$ with $J_{\perp} \ll J$, computed in a

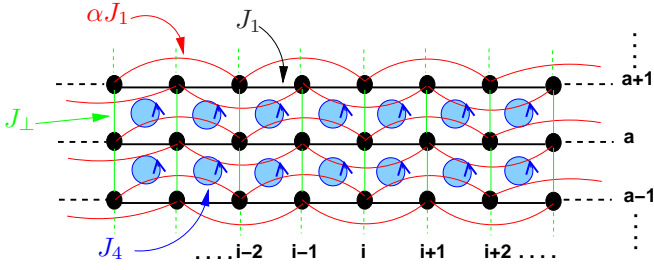


Fig. 1. Schematic picture of a system of coupled frustrated spin- $\frac{1}{2}$ chains governed by Eq. (1).

self-consistent way

$$h_{i,a} = J_{\perp} (\langle S_{i,a+1}^z \rangle + \langle S_{i,a-1}^z \rangle). \quad (2)$$

The modulation of the nearest neighbor exchange $\delta_{i,a}$ is also computed self-consistently using

$$\delta_{i,a} = \frac{J_4}{J_1} (\langle \vec{S}_{i,a+1} \cdot \vec{S}_{i+1,a+1} \rangle + \langle \vec{S}_{i,a-1} \cdot \vec{S}_{i+1,a-1} \rangle). \quad (3)$$

This modulation term might have in fact multiple origins: although a four-spin cyclic exchange mechanism provides the most straightforward derivation of it,¹⁰ at a qualitative level, J_4 can also mimic higher-order effects in J_{\perp} ¹⁴ or the coupling to adiabatic phonons.⁹ Indeed, in that case, due to a magnetoelastic coupling, the modulations $\delta_{i,a}$ result from small displacements of the ions. The elastic energy is the sum of a local term $\frac{1}{2}K_{\parallel} \sum_{i,a} \delta_{i,a}^2$ and an interchain contribution $K_{\perp} \sum_{i,a} \delta_{i,a} \delta_{i,a+1}$ of electrostatic origin.¹⁵ Then, the mean-field equation (3) is replaced by⁸

$$K_{\parallel} \delta_{i,a} + K_{\perp} (\delta_{i,a+1} + \delta_{i,a-1}) = J_1 \langle \vec{S}_{i,a} \cdot \vec{S}_{i+1,a} \rangle, \quad (4)$$

giving very similar results¹⁶ so that we can restrict ourselves to Eq. (3) without loss of generality. We first con-

sider the clean undoped system where the M chains becomes equivalent (see Fig. 1). By solving the self-consistency conditions Eqs. (2-3) using ED on finite chains with up to 16 sites¹⁷ (supplemented by a finite size scaling analysis), the transition lines $J_{\perp} = J_{\perp}(\alpha, J_4)$ separating the dimerized SP phase ($h_{i,a} = 0$) and the AF ordered phase ($h_{i,a} \neq 0$) have been obtained.^{10,18} The phase diagram is shown in Fig. 2. If the chains are not dimerized, $\delta J_{i,a}$ is constant and the exchange is just renormalised. On the other hand, if the SP phase is stable, each chain displays the same dimerized pattern when $J_4 < 0$ whereas dimer order is staggered in the transverse direction when $J_4 > 0$. Note that, apart from special features (see below), physical properties for positive or negative J_4 are quite similar. Note also that the dimerized GS would be 2^M -fold degenerate when $J_4 = 0$ (each chain is independently two-fold degenerate) while the degeneracy is reduced to 2 when $J_4 \neq 0$. When $\alpha = J_{\perp} = 0$ but $J_4 \neq 0$ each chain spontaneously dimerizes and a gap opens up. Consequently, a finite value of the AF interchain coupling is necessary to drive the system into the AF ordered phase.¹⁹ The frustration α stabilizes further the dimerized phase with respect to the AF one, the critical $J_{\perp}(\alpha)$ increasing with increasing α as seen from the phase diagram shown in Fig. 2.

3. Impurity effects

Let us now turn to the doped case. A non-magnetic dopant is described here as an inert site decoupled from its neighbors. Under doping the system becomes non-homogeneous so that the MF equations are solved self-consistently on finite $L \times M$ clusters and lead to a non-uniform solution. At each step of the MF iteration procedure, we use Lanczos ED techniques to treat *exactly* (although independently) the M *non-equivalent* finite chains and compute $\langle S_{i,a}^z \rangle$ for the next iteration step until the convergence is eventually achieved.

3.1 One impurity: soliton confinement

We first consider the case of a single dopant. Whereas in the case $J_4 = 0$ the soliton remains de-confined, a very small $J_4 \neq 0$ is sufficient to produce a confining string which binds the soliton to the dopant.¹⁰ In order to describe quantitatively the confinement mechanism near the dopant, we can define a confinement length in the chain direction ξ_{\parallel} as

$$\xi_{\parallel} = \frac{\sum_i i |\langle S_i^z \rangle|}{\sum_i |\langle S_i^z \rangle|}, \quad (5)$$

We have calculated it for a 16×8 system with $\alpha = 0.5$ and $J_{\perp} = 0.1$, and we show its variation as a function of J_4 in Fig.3. Note that $\xi_{\parallel}(J_4) \neq \xi_{\parallel}(-J_4)$ and a power law⁵ with different exponents η is expected when $J_4 \rightarrow 0$. A fit gives $\eta \sim 0.33$ if $J_4 < 0$ and $\eta \sim 0.50$ for $J_4 > 0$ (Fig.3). This asymmetry can be understood from opposite renormalisations of J_1 for different signs of J_4 . Indeed, if $J_4 < 0$ then $\delta J_{i,a} > 0$ and the nearest neighbor MF exchange becomes larger than the bare one. Opposite effects are induced by $J_4 > 0$.

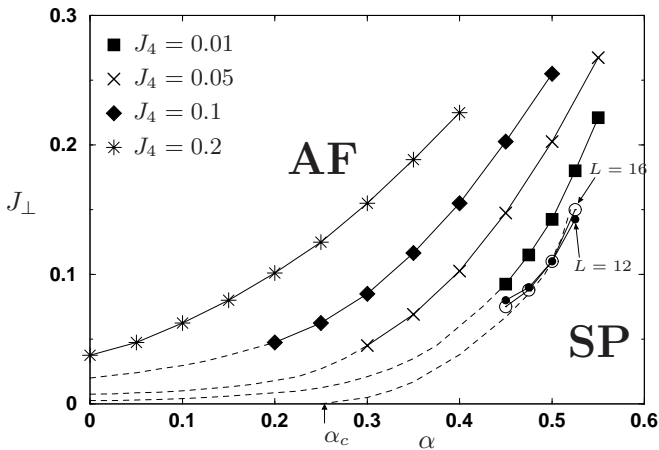


Fig. 2. SP-AF phase diagram in the (α, J_{\perp}) plane from ED of chains of length up to 16 sites. Symbols correspond to different values of $J_4 \geq 0$ as indicated on plot. Typically, finite size effects (FSE) are smaller than the size of the symbols. The computed transition lines are extended by *tentative* transition lines (dashed lines) in the region where FSE become large. At $J_4 = 0$ we have plotted a few points in the vicinity of the MG point for $L = 12$ and $L = 16$. (Figure reprinted from Ref.¹⁰).

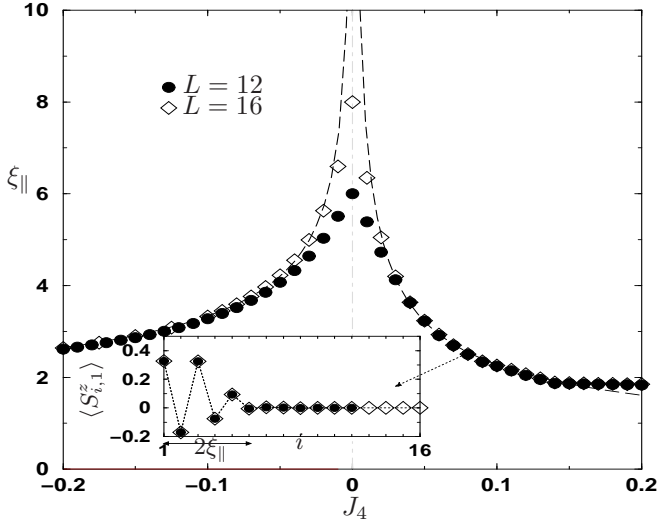


Fig. 3. ED data of the soliton average position vs J_4 calculated for $\alpha = 0.5$ and $J_\perp = 0.1$. Different symbols are used for $L \times M = 12 \times 6$ and 16×8 clusters. The long-dashed line is a power-law fit (see text). Inset shows the magnetization profile in the doped ($a = 1$) chain at $J_4 = 0.08$, ie $\xi_\parallel \simeq 2.5$ (Figure reprinted from Ref.¹⁰).

3.2 Two impurities: effective interaction

We now turn to the investigation of the effective interaction between dopants. Each impurity releases an effective spin $\frac{1}{2}$, localized at a distance $\sim \xi_\parallel$ from it due to the confining potential set by J_4 . When two impurities are introduced in the system of coupled chains (see Fig. 4), we can define an effective pairwise interaction J^{eff} as the energy difference of the $S = 1$ and the $S = 0$ ground state (GS). When $J^{\text{eff}} = E(S = 1) - E(S = 0)$ is positive (negative) the spin interaction is AF (ferromagnetic). Let us first consider the case of two dopants in

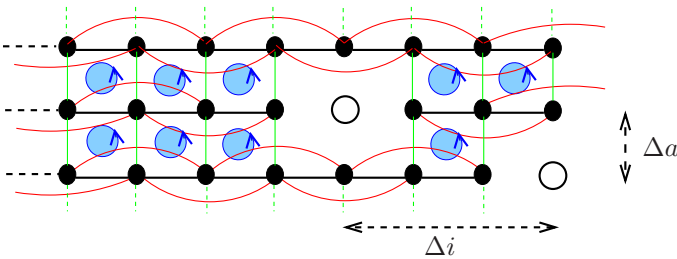


Fig. 4. Schematic picture of the system of coupled frustrated spin- $\frac{1}{2}$ chains doped with two non magnetic impurities separated by a distance Δi (resp. Δa) in the chains direction (resp. transverse direction).

the same chain. (i) When the two vacancies are on the same sub-lattice the moments experience a very small ferromagnetic $J^{\text{eff}} < 0$ as seen in Fig. 5 with $\Delta a = 0$ so that the two effective spins $\frac{1}{2}$ are almost free. (ii) When the two vacancies sit on different sub-lattices, Δi is odd and the effective coupling is AF with a magnitude close to the singlet-triplet gap. Fig. 5 with $\Delta a = 0$ shows that the decay of J^{eff} with distance is in fact very slow

for such a configuration. The behavior of the pairwise interaction of two dopants located on *different* chains ($\Delta a = 1, 2, 3$) is shown in Fig. 5 for $\Delta a = 1, 2, 3$ for $J_4 > 0$. When dopants are on opposite sub-lattices the effective interaction is antiferromagnetic. At small dopant separation $J^{\text{eff}}(\Delta i)$ increases with the dopant separation as the overlap between the two AF clouds increases until $\Delta i \sim 2\xi_\parallel$. For larger separation, $J^{\text{eff}}(\Delta i)$ decays rapidly. If dopants are on the same sub-lattice, solitons are located on the same side of the dopants and the effective exchange $J^{\text{eff}}(\Delta i)$ is ferromagnetic and decays rapidly to become negligible when $\Delta i > 2\xi$. The key feature here is the fact that the effective pairwise interaction is *not* frustrating (because of its sign alternation with distance) although the frustration is present in the microscopic underlying model. Our next step is to fit the numerical data

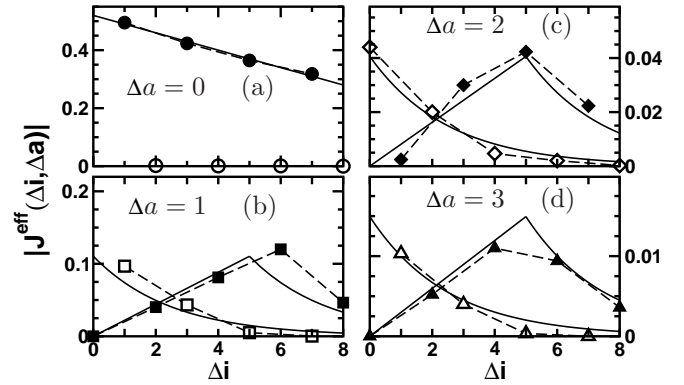


Fig. 5. Magnitude of the effective magnetic coupling between two impurities located either on the same chain (a) or on different ones (b-c-d) vs the dopant separation Δi in a system of size $L \times M = 16 \times 8$ with $\alpha = 0.5$, $J_\perp = 0.1$, and $J_4 = 0.08$. Closed (resp. open) symbols correspond to AF (F) interactions. Full lines are fits (see text). (Figure reprinted from Ref.¹⁸).

in order to derive an analytic expression for J_{eff} . Using only five parameters, two energy scales and three length scales, we can fit ED data with very simple mathematical expressions. When $\Delta a = 0$ (same chain), J^{eff} approximately fulfills $J^{\text{eff}}(\Delta i, 0) = J_0(1 - \Delta i/\xi_\parallel^0)$ for Δi even and $\Delta i < \xi_\parallel^0$, and $J^{\text{eff}}(\Delta i, 0) = 0$ otherwise. For dopants located on different chains and on the same sub-lattice ($\Delta i + \Delta a$ even) one has,

$$J^{\text{eff}}(\Delta i, \Delta a) = -J'_0 \exp\left(-\frac{\Delta i}{\xi_\parallel}\right) \exp\left(-\frac{\Delta a}{\xi_\perp}\right), \quad (6)$$

while if the dopants are on opposite sub-lattices, one gets

$$J^{\text{eff}}(\Delta i, \Delta a) = J'_0 \frac{\Delta i}{2\xi_\parallel} \exp\left(-\frac{\Delta a}{\xi_\perp}\right) \quad (7)$$

for $\Delta i \leq 2\xi_\parallel$ and

$$J^{\text{eff}}(\Delta i, \Delta a) = -J'_0 \exp\left(-\frac{\Delta i - 2\xi_\parallel}{\xi_\parallel}\right) \exp\left(-\frac{\Delta a}{\xi_\perp}\right), \quad (8)$$

for $\Delta i > 2\xi_\parallel$. The fitting parameters are $J_0 = 0.52$, $J'_0 = 0.3$, $\xi_\parallel^0 = 17.33$, $\xi_\parallel = 2.5$ and $\xi_\perp = 1$ in the case considered here : $\alpha = 0.5$, $J_\perp = 0.1$ and $J_4 = 0.08$ (see Fig.5).

4. Impurity induced antiferromagnetic ordering

In order to study the impurity induced AF ordering in the system of weakly coupled chains [Eq. (1)], a long-range *non-frustrated* effective model of diluted effective spin- $\frac{1}{2}$ is defined,

$$\mathcal{H}^{\text{eff}} = \sum_{\mathbf{r}_1, \mathbf{r}_2} \epsilon_{\mathbf{r}_1} \epsilon_{\mathbf{r}_2} J^{\text{eff}}(\mathbf{r}_1 - \mathbf{r}_2) \mathbf{S}_{\mathbf{r}_1} \cdot \mathbf{S}_{\mathbf{r}_2}, \quad (9)$$

with $\epsilon_{\mathbf{r}} = 1$ (0) with probability x ($1-x$), where x is the dopant concentration. Such a model can be studied by Quantum Monte Carlo (QMC) simulations on $L_x \times L_y$ clusters much larger than those accessible to ED⁹ and *at all temperatures*.

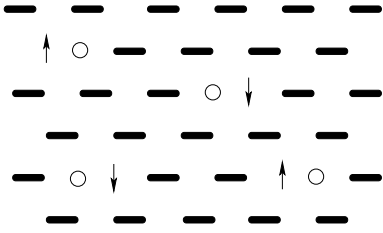


Fig. 6. Schematic picture of a doped SP system. Thick bonds correspond to dimers, and non-magnetic dopants (released spin- $\frac{1}{2}$) are represented by open circles (arrows).

We study the effective Heisenberg model using the powerful Stochastic Series Expansion (SSE) method²⁰ to investigate GS as well as finite T properties. In this approach, the interactions are sampled stochastically, and for a long-ranged interaction the computational effort is then reduced from $\sim N_s^2$ to $N_s \ln(N_s)$.²¹ In order to accelerate the convergence of the simulations at the very low temperatures needed to study the ground state, we use a β -doubling scheme²² where the inverse temperature is successively increased by a factor 2. Comparing results at several $\beta = 2^n$, one can subsequently check that the $T \rightarrow 0$ limit has been reached.

4.1 $T = 0$ antiferromagnetic ordering

The AF ordering instability is signalled by the divergence with system size of the staggered structure factor,

$$S(\pi, \pi) = \frac{1}{L_x L_y} \langle (\sum_i (-1)^i S_i^z)^2 \rangle. \quad (10)$$

Note that within our effective model approach, only the sites carrying a ‘‘dopant spin’’ contribute to this sum. It is convenient to normalize S with respect to the number of sites, i.e. to define a staggered structure factor per site; $s(\pi, \pi) = S(\pi, \pi)/L_x L_y$. In an ordered AF state, $s(\pi, \pi)$ should converge, with increasing size, to a non-zero value $< 1/4$. The (finite size) sublattice magnetization m_{AF} can then be obtained by averaging $s(\pi, \pi)$ over a large number of dopant distributions, i.e. $(m_{\text{AF}})^2 = 3 \langle s(\pi, \pi) \rangle_{\text{dis}}$, where the factor 3 comes from the spin-rotational invariance²³ and $\langle \dots \rangle_{\text{dis}}$ stands for the disorder average. The staggered magnetization per dopant is then simply $m_{\text{spin}} = m_{\text{AF}}/x$. Since, strictly

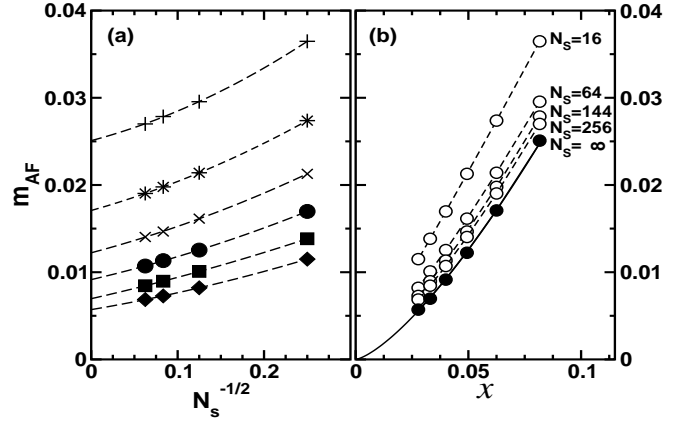


Fig. 7. Staggered magnetization per site. Disorder average has been done over at least 2000 samples. (a) Finite size extrapolations (see text) at fixed doping x . The different symbols are used for different concentrations x with, from top to bottom, $x = 4/49, 0.0625, 4/81, 0.04, 4/121, 1/36$. (b) Doping dependence of m_{AF} for various numbers of spins and in the thermodynamic limit (full symbols). (Figure reprinted from Ref.¹¹)

speaking, in 2D the divergence of $S(\pi, \pi)$ occurs only at $T = 0$ ($\beta = \infty$) it is appropriate to first extrapolate the finite size numerical data to $T = 0$, and then using a polynomial fit in $1/\sqrt{N_s}$ an accurate extrapolation to the thermodynamic limit is performed as shown in Fig.7(a). The doping dependence of the extrapolated m_{AF} is given in Fig.7(b). We have tested various fits to the data. Assuming a power law $\propto x^\mu$, the best fit (solid line in Fig.7(b)) gives an exponent $\mu \simeq 1.38 > 1$.

4.2 Néel temperature

It is also very instructive to calculate the Néel temperature, assuming a small (effective) 3D magnetic coupling λ_{3D} between the 2D planes. Using an RPA criterion, the critical temperature T_N is simply given by $\chi_{\text{stag}}(T_N) = 1/|\lambda_{3D}|$ where the staggered spin susceptibility (normalized per site) is defined as usual by,

$$\chi_{\text{stag}}(T) = \frac{1}{L^2} \sum_{i,j} (-1)^{r_i+r_j} \int_0^\beta d\tau \langle S_i^z(0) S_j^z(\tau) \rangle, \quad (11)$$

and averaged over several disorder configurations (typically 2000). Since $\chi_{\text{stag}}(T_N)$ is expected to reach its thermodynamic limit for a *finite* linear size L as long as T_N remains *finite*, accurate values of T_N can be obtained using a finite size computation of $\chi_{\text{stag}}(T)$ for not too small inter-chain couplings. Fig. 8(a) shows that $\chi_{\text{stag}}(T)$ diverges when $T \rightarrow 0$. T_N is determined by the intersection of the curve $\chi_{\text{stag}}(T)$ with an horizontal line at coordinate $1/\lambda_{3D}$. Note that finite size corrections remain small, even in the worst case corresponding to very small λ_{3D} values and large dopant concentrations. The doping dependence of T_N is plotted in Fig. 8(b) for a particularly small value $\lambda_{3D} = 0.01$ (in order to show the small size dependence observable in that case). It clearly reveals a rapid decrease of T_N when $x \rightarrow 0$, but, in agreement with experiments, does not suggest a non-zero critical concentration. In Fig.8(b), we show the behavior of $T_N(x)$ down to $x \simeq 0.007$. Note that from numerical fits of the data,

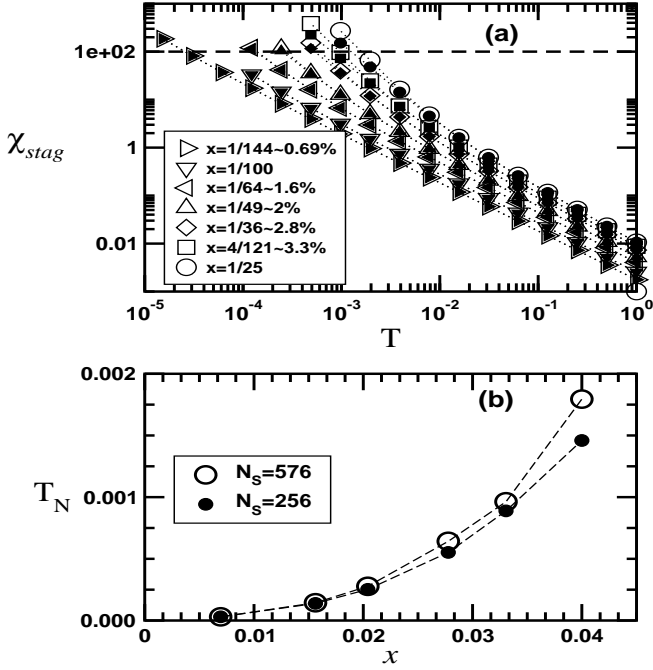


Fig. 8. (a) Staggered susceptibility of a 2D layer vs temperature (using log-log scales) for $N_s = 256$ (full symbols) and $N_s = 576$ (open symbols) spins. Concentrations x are shown on the plot. $\lambda_{3D}^{-1} = 100$ is shown by the dashed line. (b) Néel temperature vs dopant concentration x for a 3D RPA inter-plane coupling $\lambda_{3D} = 0.01$ and for $N_s = 256$ and $N_s = 576$ spins. (Figure reprinted from Ref.¹¹)

we can not clearly distinguish between a power-law behavior (with an exponent ~ 2.5) and an exponential law like $A \exp(-B/x)$, as suggested by fits of experimental data for $\text{Cu}_{1-x}\text{Zn}_x\text{GeO}_3$.²⁴

5. Low temperature critical properties

5.1 Saturation of the Curie constant

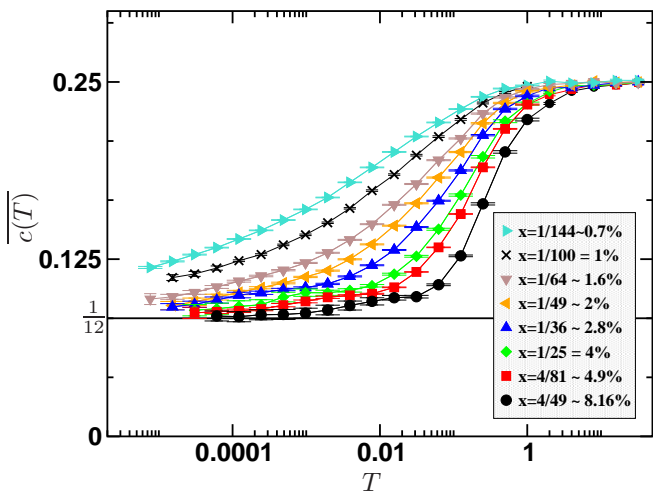


Fig. 9. Curie constant per spin (C) plotted vs the energy scale. Quantum Monte Carlo SSE results shown vs T for $N_s = 256$ spins and 9 different concentrations x indicated on the plot. Disorder is performed over 10^3 to 10^4 samples. (Figure reprinted from Ref.¹²).

As a first investigation, we have computed the uniform susceptibility $\chi(T)$ for a wide range of temperatures using SSE simulations. Results for the Curie constant $C(T) = T\chi(T)$ are shown in Fig. 9. At the highest temperatures the effective dopant spins behave as free spins while at low temperature we observe a new Curie-like behavior with a reduced Curie constant $\sim 1/12$. Although here the 2D system orders at $T = 0$ (as proven above) this behavior agrees with a qualitative argument based on the formation of large spin clusters due to the presence of AF as well as ferromagnetic (F) couplings, applied by Sigrist and Furusaki²⁵ in the 1D case.

5.2 Real Space Renormalization Group

In order to explore this large spin formation, we follow the pioneering work of Ma, Dasupta and Hu²⁶ and also Bhatt and Lee,²⁷ and extend the Real Space Renormalization Group (RSRG) scheme to hamiltonian (9) with F and AF long-distance couplings. It turns out that such a RSRG procedure has allowed the identification of the so-called *Infinite Randomness Fixed point* (IRFP) by D. Fisher for the disordered Heisenberg spin- $\frac{1}{2}$ chain²⁸ as well as for the Ising chain in transverse field at criticality.²⁹ Nevertheless, such an IRFP (as well as its associated *random Singlet Phase*) is unstable against the introduction of randomness in the couplings' signs, as shown first by Westerberg *et al.*³⁰ for the Heisenberg spin- $\frac{1}{2}$ chain with random couplings in magnitude *and* sign. The new fixed point identified in the 1D case, using an extended RSRG scheme³¹ and checked numerically using QMC simulations,³² is especially characterized by a large spin formation.³³

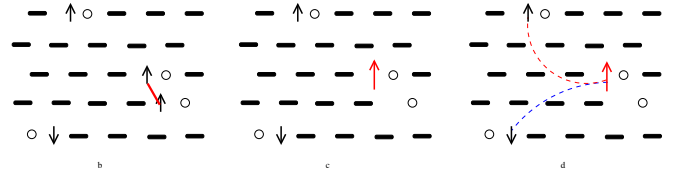


Fig. 10. Schematic picture of one RG step performed in the doped spin-Peierls system. Thick bonds stand for dimers and non-magnetic impurities (released spins $\frac{1}{2}$) are represented by open circles (black arrows). The initial RSRG step is illustrated starting from a typical configuration with 4 impurities: (a) The strongest coupled pair is identified (red line). (b) This pair, e.g. ferromagnetic here, is replaced by a spin $S = 1$ (red arrow). (c) The couplings with all other spins (dashed lines) are renormalized.

In the 2D problem addressed here, long range interactions with random sign and magnitude can also be studied by an extended version of the RSRG technique. Let us first define the effective interaction as $J_{i,j}$ where i and j label the *randomly distributed spins* and run from 1 to N_s . One single RG step is described as follows (see Fig. 10): 1) Identify the most strongly coupled pair of spins (S_1, S_2) i.e. with the largest energy gap $\Delta_{1,2}$, $\Delta_{1,2} = J_{1,2}(1 + |S_1 - S_2|)$ if $J_{1,2} > 0$ (AF) and $\Delta_{1,2} = -J_{1,2}(S_1 + S_2)$ if $J_{1,2} < 0$ (F). Note that $\Delta_{1,2}$ defines the energy scale of the transformation which will,

in fact, play the role of the temperature. 2) Replace it by an effective spin $S' = |S_1 - S_2|$ if the coupling is AF or $S' = S_1 + S_2$ in the F case. 3) Renormalize all the magnetic couplings with the following rules : (i) If $S' \neq 0$, as given by a first order perturbation theory, the new couplings between S' and all the other spins (S_3, S_4, \dots, S_{N_s}) are set to

$$\tilde{J}_{(S', S_i)} = J_{1,i} c(S_1, S_2, S') + J_{2,i} c(S_2, S_1, S'), \quad (12)$$

with

$$c(S_1, S_2, S') = \frac{S'(S' + 1) + S_1(S_1 + 1) - S_2(S_2 + 1)}{2S'(S' + 1)}. \quad (13)$$

(ii) If $S' = 0$, the pair (S_1, S_2) is frozen. Using a cluster approximation²⁷ that involves only the extra pair (S_3, S_4) the most strongly coupled to S_1 and S_2 and a second order perturbation, the coupling $J_{3,4}$ is renormalized as

$$\tilde{J}_{3,4} = J_{3,4} + \frac{2S_1(S_1 + 1)}{3J_{1,2}}(J_{1,3} - J_{2,3})(J_{2,4} - J_{1,4}). \quad (14)$$

The same procedure is then reiterated. We also check that the RSRG preserves the non-frustrated character of the problem.

5.3 Large spin formation

Due to the presence of both F and AF couplings, clusters with large effective spins are created during the procedure similarly to what occurs in the 1D random F-AF spin- $\frac{1}{2}$ chain.³⁰ At each RG step, the energy scale Δ_0 decreases and both the number of inactive spins frozen into singlets and the number of clusters build from a large number n correlated spins- $\frac{1}{2}$, increase. The aforementioned random walk argument predicts that, the average number $\langle n \rangle$ of spins- $\frac{1}{2}$ inside clusters and their average spin magnitude $\langle S^{\text{eff}} \rangle$ should be related by $\langle S^{\text{eff}} \rangle \sim \langle n \rangle^{1/2}$ at low enough temperatures. Therefore we expect the effective spin of these clusters to grow monotonously as the energy scales down. We have analyzed this process using the RSRG scheme to compute both $\langle S^{\text{eff}} \rangle$ and $\langle n \rangle$ as a function of $\langle \Delta_0 \rangle$. This is shown in Fig. 11 which clearly demonstrates the formation of large moments. Moreover, power-law divergences like

$$\langle S^{\text{eff}} \rangle \sim \langle \Delta_0 \rangle^{-\alpha(x)} \quad \text{and} \quad \langle n \rangle \sim \langle \Delta_0 \rangle^{-\kappa(x)} \quad (15)$$

are observed with $\kappa \simeq 2\alpha$. Interestingly enough, we find that α depends on x , like $\sim \sqrt{x}$, in contrast to the random F-AF spin chain for which $\alpha = 0.22 \pm 0.01$.^{?,31,32}

The Curie constant can also be evaluated using the decimation procedure. The RSRG computation of C is performed, at each RG step, using the formula $C = \frac{1}{3N_s} \sum_{\sigma} N_{\sigma} \sigma(\sigma + 1)$ where N_{σ} is the number of active effective spins of size σ , the data being then averaged over disorder. We have also checked that finite size effects are negligible when $N_s \geq 256$ and we have chosen $N_s = 1024$ in most computations. Fig. 12 shows results for the Curie constant per spin obtained with the decimation procedure. We can confront the RSRG results to QMC data obtained on the same model and for the same parameters. We observe a qualitative agreement between

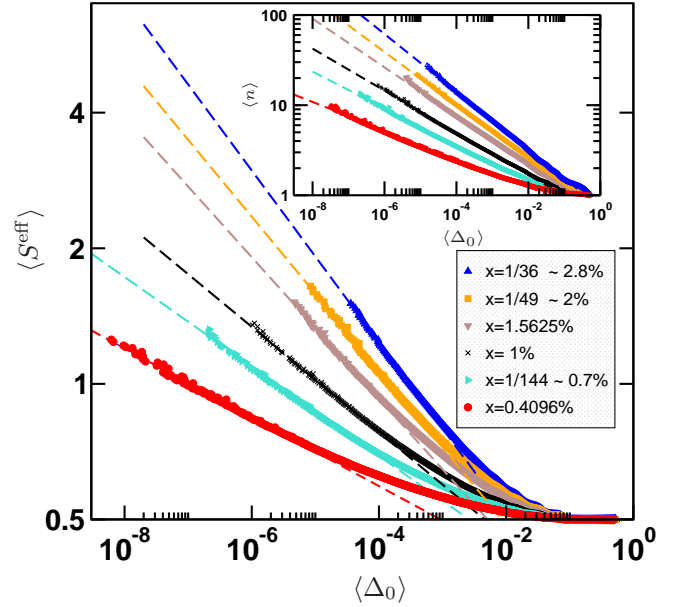


Fig. 11. Average effective spin $\langle S^{\text{eff}} \rangle$ of the clusters of active spins vs the energy scale $\langle \Delta_0 \rangle$ for six different concentrations x indicated on the plot. Numerical RSRG data obtained for $N_s = 1024$ spins over more than 10^4 samples. Inset: for the same samples, average number $\langle n \rangle$ of initial spins- $\frac{1}{2}$ per cluster vs $\langle \Delta_0 \rangle$. Dashed lines are power-law fits (see text). (Figure reprinted from Ref.¹²).

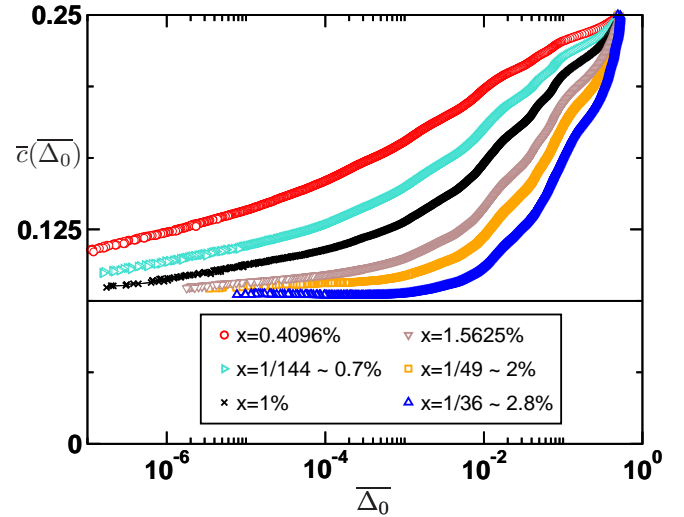


Fig. 12. Curie constant per spin $\langle C \rangle$ plotted vs the energy scale. Numerical RSRG results shown for $N_s = 1024$ spins and 6 different concentrations x as indicated on the plot, vs the RG energy scale $\langle \Delta_0 \rangle$. Error bars are typically smaller than symbol sizes, the number of samples always exceeding 10^4 . The full line correspond to the saturation value of $1/12$. (Figure reprinted from Ref.¹²).

Fig.9 and Fig.12 where, at high temperatures, the spins behave as paramagnetic free magnetic moments (giving a Curie constant of $\frac{1}{4}$ per spin) and where saturation to $\frac{1}{12}$ is observed at low T , the spins being correlated inside large clusters. At small concentration, the agreement becomes even quantitative, as seen in the Fig.13 where a direct comparison between RSRG and SSE is shown for the six lowest values of x .

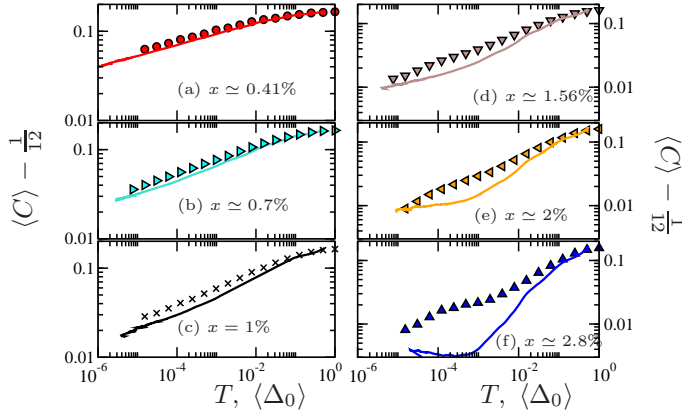


Fig. 13. Direct comparisons between RSRG (full lines) and SSE simulations (symbols) of $\langle C \rangle - 1/12$ are shown for the 6 different concentrations indicated by (a), (b), ..., (f) vs the RG energy scale $\langle \Delta_0 \rangle$ or the SSE temperature T . (Figure reprinted from Ref.¹²).

5.4 Scaling regime

We now turn to the analysis of the scaling regime. At very low temperatures, from the analogy with 1D systems we expect the following quantum corrections

$$\langle C(T) \rangle - 1/12 \sim T^\gamma, \quad (16)$$

with $\gamma = \alpha$ in 1D.³² Similarly, one expects for the staggered susceptibility (per spin),

$$\langle \chi_{\text{stag}}(T) \rangle \sim T^{-1-2\gamma'}. \quad (17)$$

In 1D, γ' is expected to be equal to α ,³⁵ but in the present case, by direct fits of the low T (see Fig. 14), we found

$$\gamma' \simeq \gamma \simeq 2\alpha.$$

Thoses exponents are plotted in Fig. 15. An overall very

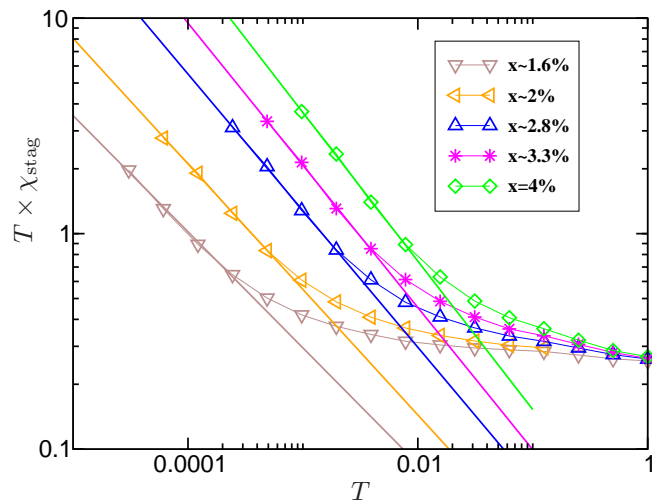


Fig. 14. $T \langle \chi_{\text{stag}}(T) \rangle$ plotted vs T for five different concentrations. Full lines are fits corresponding to power-law behaviors $\sim T^{-2\gamma'}$. All data are computed by QMC using $N_s = 256$ random spins and averaged over disorder. (Figure reprinted from Ref.¹²).

good agreement is seen between the different methods, in particular between the estimates of γ obtained from

the analysis of the Curie constant computed by QMC and RSRG. We stress again that the exponent α deduced from the analysis of the change of cluster sizes and spins is roughly a factor of 2 smaller than γ . Interestingly enough, $\gamma \simeq 2\alpha \propto \sqrt{x}$ in all cases.

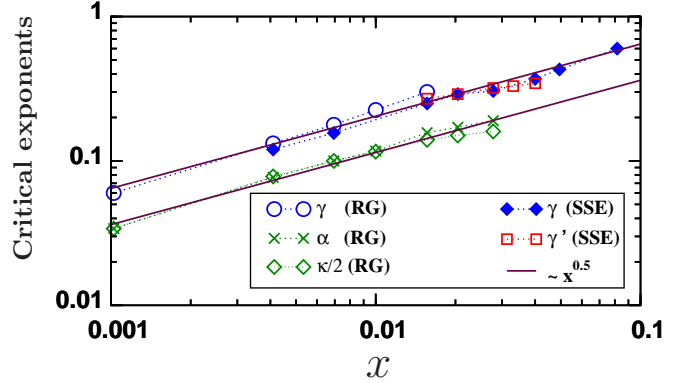


Fig. 15. Exponents $\alpha(x)$, $\gamma(x)$ and $\gamma'(x)$ extracted from various SSE and RSRG data as indicated on the plot (see text for details). Straight lines are $\sim \sqrt{x}$. (Figure reprinted from Ref.¹²).

It is remarkable that such properties are observed above the $T = 0$ ordered magnetic groundstate. Moreover, it is the first example of a two-dimensional random magnet exhibiting a large spin phase with a disorder (the concentration x) dependence of the critical exponents. Whereas doped CuGeO₃ might be a good candidate for the experimental observation of a critical regime, the so large three-dimensional ordering temperature prevents such an observation. More strongly diluted samples are necessary to reach the scaling regime.

6. Conclusion

Starting from a microscopic model for impurity-doped dimerized and frustrated coupled spin-chains (similar to let's say, Zn-doped copper germanate), we have derived a simple and tractable effective model describing $S=1/2$ effective spins interacting through long range (spatially anisotropic) interactions. An important property of this long-range exchange is its oscillating nature (with both AF and F couplings) in such a way it is essentially non-frustrating, hence leading to an AF instability at low temperature (in the presence of a small 3D coupling). This is a remarkable fact since magnetic ordering in the pure system is prevented by frustration. Using state-of-the-art SSE QMC computations thermodynamic properties of the effective model are studied in details down to very low temperatures. Critical behaviors with impurity concentration-dependent exponents are found and interpreted using a new Real Space RG procedure clearly establishing the important role of large clusters of correlated spins carrying a finite magnetization.

Acknowledgment

We are deeply grateful to A.W. Sandvik and M. Sigrist for many useful discussions and some collaborations. We also thank IDRIS (Orsay, France) for allocation of CPU

time on their supercomputers. N.L. thanks I. Affleck for hospitality at UBC.

- 1) M. Hase, I. Terasaki, and K. Uchinokura, Phys. Rev. Lett. **70**, 3651 (1993).
- 2) M. Hase et al., Phys. Rev. Lett. **71**, 4059 (1993).
- 3) S.B. Oseroff et al., Phys. Rev. Lett. **74**, 1450 (1995); L.-P. Regnault et al., Europhys. Lett. **32** 579 (1995); T. Masuda et al., Phys. Rev. Lett. **80**, 4566 (1998); B. Grenier et al., Phys. Rev. B **58**, 8202 (1998).
- 4) E. S. Sørensen, I. Affleck, D. Augier, and D. Poilblanc, Phys. Rev. B. **58**, R14701 (1998).
- 5) T. Nakamura, Phys. Rev. B **59**, R6589 (1999).
- 6) B. Normand and F. Mila, Phys. Rev. B. **65**, 104411 (2002).
- 7) G. B. Martins, E. Dagotto and J. Riera, Phys. Rev. B. **54**, 16032 (1996).
- 8) P. Hansen, D. Augier, J. Riera, and D. Poilblanc, Phys. Rev. B. **59**, 13557 (1999).
- 9) A. Dobry, P. Hanse, J. Riera, D. Augier and D. Poilblanc, Phys. Rev. B. **60**, 4065 (1999).
- 10) N. Laflorencie and D. Poilblanc, Phys. Rev. Lett. **90**, 157202 (2003).
- 11) N. Laflorencie, D. Poilblanc and A. W. Sandvik, Phys. Rev. B **69**, 212412 (2004).
- 12) N. Laflorencie, D. Poilblanc and M. Sigrist, Phys. Rev. B (in press); cond-mat/0405417.
- 13) H. J. Schulz, Phys. Rev. Lett. **77**, 2790 (1996); see also A.W. Sandvik, Phys. Rev. Lett. **83**, 3069 (1999).
- 14) T.M.R. Byrnes, M.T. Murphy and O.P. Sushkov, Phys. Rev. B. **60**, 4057 (1999).
- 15) I. Affleck, Proceedings of the NATO ASI: Dynamical properties of Unconventional Magnetic Systems, April 1997, cond-mat/9705127 (unpublished).
- 16) In fact, for the *undoped* system, an *exact* mapping exists assuming $2J_4/J = J/K_{\text{eff}}$ where $K_{\text{eff}} = K_{\parallel} - 2|K_{\perp}|$.
- 17) For more details about the numerical procedure, see.¹⁸
- 18) N. Laflorencie and D. Poilblanc, Lect. Notes Phys. **645**, 227-252 (2004).
- 19) For numerical studies on anisotropic dimerized square lattice see M. Matsumoto, C. Yasuda, S. Todo, and H. Takayama, Phys. Rev. B. **65**, 014407 (2002) and references therein.
- 20) A. W. Sandvik, Phys. Rev. B **59**, R14157 (1999).
- 21) A. W. Sandvik, Phys. Rev. E **68**, 056701 (2003).
- 22) A. W. Sandvik, Phys. Rev. B **66**, 024418 (2002).
- 23) J. D. Reger and A. P. Young, Phys. Rev. B **37**, 5978 (1988).
- 24) K. Manabe et al., Phys. Rev. B **58**, R575 (1998).
- 25) For related studies of a doped spin ladder with *no frustration* see M. Sigrist and A. Furusaki, J. Phys. Soc. Jpn **65**, 2385 (1996).
- 26) S. Ma, C. Dasgupta and S. Hu, Phys. Rev. Lett. **43**, 1434 (1979).
- 27) R. N. Bhatt and P. A. Lee, Phys. Rev. Lett. **48**, 344 (1982).
- 28) D. S. Fisher, Phys. Rev. B **50**, 3799 (1994).
- 29) D. S. Fisher, Phys. Rev. Lett. **69**, 534 (1992); Phys. Rev. B **51**, 6411 (1995).
- 30) E. Westerberg, A. Furusaki, M. Sigrist and P. A. Lee, Phys. Rev. Lett. **75**, 4302 (1995); A. Furusaki, M. Sigrist, E. Westerberg and P. A. Lee, Phys. Rev. B **52**, 15930 (1995).
- 31) E. Westerberg, A. Furusaki, M. Sigrist and P. A. Lee, Phys. Rev. B **55**, 12578 (1997).
- 32) B. Frischmuth and M. Sigrist, Phys. Rev. Lett. **79**, 147 (1997); B. Frischmuth *et al.*, Phys. Rev. B **60**, 3388 (1999).
- 33) It turns out that such a large spin phase (LSP) seems to appear more generally in a large class of frustrated spin systems with random exchange, see Y.-C. Lin, R. Mélin, H. Rieger and F. Iglói, Phys. Rev. B **68**, 024424 (2003).
- 34) Note however that the universality class identified in³⁰ as a RG fixed point occurs only for initial gap distributions less singular than $P_c(\Delta) \sim \Delta^{-y_c}$, with $0.65 \lesssim y_c \lesssim 0.75$. For more singular distributions, as it is the case here, critical exponents are not universal anymore, at least in 1D.³¹
- 35) N. Nagaosa *et al.*, J. Phys. Soc. Japan **65**, 3724 (1996).